ELSEVIER

Polymer 43 (2002) 3879–3890

polymer

www.elsevier.com/locate/polymer

Preparation and characterization of polyvinylidene fluoride hollow fiber membranes for ultrafiltration

M. Khayet[a,*], C.Y. Feng[b], K.C. Khulbe[b], T. Matsuura[b,1]

[a]*Department of Applied Physics I, Faculty of Physics, University Complutense of Madrid, Av. Complutense s/n, 28040 Madrid, Spain*
[b]*Department of Chemical Engineering, Industrial Membrane Research Institute, University of Ottawa, 161 Louis Pasteur, P.O. Box 450, Stn. A, Ottawa, Ont., Canada K1N 6N5*

Received 17 October 2001; received in revised form 21 January 2002; accepted 5 April 2002

Abstract

Polyvinylidene fluoride (PVDF) hollow fiber membranes were prepared using the solvent spinning method. *N*,*N*-dimethylacetamide was the solvent and ethylene glycol was employed as non-solvent additive. The effect of the concentration of ethylene glycol in the PVDF spinning solution as well as the effect of ethanol either in the internal or the external coagulant on the morphology of the hollow fibers was investigated. The prepared membranes were characterized in terms of the liquid entry pressure of water measurements, the gas permeation tests, the scanning electron microscopy, the atomic force microscopy, and the solute transport experiments. Ultrafiltration experiments were conducted using polyethylene glycol and polyethylene oxides of different molecular weights cut-off as solutes. A comparative analysis was made between the membrane characteristic parameters obtained from the different characterization techniques.

Keywords: Hollow fiber polyvinylidene fluoride membranes; Membrane preparation and characterization; Ultrafiltration

1. Introduction

Among hydrophobic polymers (e.g. polytetrafluoroethylene (PTFE) and polypropylene (PP)), polyvinylidene fluoride (PVDF) is, so far, the only polymer that can be used for the preparation of asymmetric membranes. It is one of the polymers that are thermally stable, possess good chemical resistance, and are resistant to most of corrosive chemicals and organic compounds. Hence, PVDF has been a subject of active research in polymer science and has received increasing attention for various membrane separation applications such as membrane distillation, pervaporation, gas separation, and ultrafiltration [1–5].

Although an extensive series of studies have been carried out to improve the properties of PVDF membranes, most of them are related to flat sheet membranes prepared by the dry/wet phase inversion method. On the other hand, less research has been conducted on the fabrication and characterization of PVDF hollow fiber membranes. This may be due to the fact that the preparation of hollow fiber membranes is a complicated process involving various factors such as the rapid phase inversion kinetics and the interfacial mass transfer during the spinning process, as well as the large number of spinning parameters (e.g. linear extrusion rate, air gap, wind-up speed, nature of the internal and the external coagulants, polymer dope viscosity, etc.). In addition, during the formation of the fibers, simultaneous internal and external coagulation processes may take place.

It has been reported that the properties of PVDF membranes could be improved by introducing non-solvent additives in the polymer solution. As far as we know, the non-solvents tested are polyvinylpyrrolidone (PVP) [6,7], polyethylene glycol (PEG) [8], polystyrene sulfonic acid [9], ethanol [10], lithium chloride (LiCl) [2,5], mixtures of LiCl/water and LiCl/1-propanol [11], water [12], glycerol and phosphoric acid [13]. In this work, an attempt is made to include ethylene glycol into the list of the non-solvent additives that are incorporated into the PVDF solution for pore making and to improve the PVDF membrane performance.

It has also been shown that the nature of the liquid coagulant is important in determining the morphology of asymmetric PVDF membranes. The coagulants studied were water, alcohols, mixtures of water with various alcohols or with various solvents [14]. Bottino et al. [15] studied the effect of different solvents on the structure of

* Corresponding author. Tel.: +34-91-3944454; fax: +34-91-3945191.
E-mail addresses: khayetm@eucmax.sim.ucm.es (M. Khayet), matsuura@eng.uottawa.ca (T. Matsuura).
[1] Tel.: +1-613-5625800x6114; fax: +1-613-5625172.

0032-3861/02/$ - see front matter
PII: S0032-3861(02)00237-9

Nomenclature

Symbols

a_d	Einstein–Stokes diameter (cm)
B	gas permeance (mol/m^2 s Pa)
C_f	solute concentration in the feed (ppm)
C_p	solute concentration in the permeate (ppm)
d_p	pore size (nm)
f_i	fraction of pores of diameter d_i
i	number of the measured pores by AFM
J	total solvent flux through the membrane (m^3/m^2 s)
I_0	intercept defined in Eq. (2) (mol/m^2 s Pa)
L_x, L_y	dimensions of the surface $f(x,y)$ (nm)
L_p	effective pore length (m)
LEPw	liquid entry pressure of water (kPa)
M	molecular weight (kg/kmol)
n	total number of measured pores by AFM
N	pore density (μm^{-2})
N_p	number of points in a given area
P_m	mean pressure (Pa)
PR	product permeation rate (m^3/m^2 s)
ΔP	transmembrane pressure (Pa)
r_p	pore radius (μm)
R	gas constant (J/mol K)
R_a	mean roughness (nm)
R_q	root mean square of Z data (nm)
R_z	mean difference between five highest peaks and five lowest valleys (nm)
S_0	slope defined in Eq. (2) (mol/m^2 s Pa^2)
T	absolute temperature (K)
Z_m	average of the Z values (nm)
Z_i	current Z value (nm)

Greek letters

α	solute separation (%)
χ	median rank (50%)
δ	membrane thickness (μm)
ε	membrane porosity
ε_s	surface porosity defined in Eq. (13)
ε_v	membrane porosity defined in Eq. (1)
ε/L_p	effective porosity (m^{-1})
η	solvent viscosity (N s/m^2)
μ_p	geometric mean pore size of the membrane (nm)
ν_H	maximum nodule size (nm)
ν_L	minimum nodule size (nm)
ν_m	average nodule size (nm)
ρ_m	density of the membrane (kg/m^3)
ρ_{pol}	density of the polymer material (kg/m^3)
σ_p	geometric standard deviation (nm)

PVDF flat sheet membranes, including *N*,*N*-dimethylacetamide (DMAC), dimethylformamide (DMF), *N*-methyl-2-pyrrolidone (NMP), hexamethylphosporamide (HMPA), tetramethylurea (TMU), triethylphosphate (TEP) and dimethylsulfoxide (DMSO). The effect of the external coagulant (i.e. coagulation bath), water/ethanol mixtures with ethanol contents of 10–50%, on the morphology of PVDF hollow fiber membranes was investigated, when PVP was added as a pore forming agent [6]. The presence of ethanol in the coagulation bath was believed to reduce the polymer precipitation during phase inversion process. It was found that the gas permeation flux decreased with increasing ethanol content in water to 50%. It was difficult to spin PVDF hollow fiber membranes using external coagulants with high ethanol contents, particularly when PVP was added to the casting solution. The effect of ethanol as an internal coagulant was also studied [7]. The higher gas permeation flux and water solution flux observed, when ethanol was used as an internal coagulant instead of water, were attributed to the elimination of the internal skin layer. Due to the slow internal coagulation, the wet spinning method (i.e. air gap of zero) and high flow rate of internal coagulant were necessary for spinning [7].

The present investigation is carried out to study the effects of an aqueous ethanol solution (50% v/v), when used as either internal and/or external coagulant, on the morphology of both the inner and the outer surfaces of PVDF hollow fiber membranes. The membranes so prepared were characterized by their non-wettability (liquid entry pressure of water (LEPw) measurements), porosity measurements using isopropyl alcohol, gas permeation tests, atomic force microscopy (AFM) and scanning electron microscopy (SEM) analysis. Ultrafiltration tests were conducted using PEG and polyethylene oxide (PEO) solutes of different molecular weights.

2. Experimental

2.1. Materials used for preparation of the hollow fibers

PVDF, Kynar grade 740 (Elf Autochem, Philadelphia) was used for the hollow fiber membrane material. The solvent DMAC (Synthesis Grade, Merck, >99%) was employed to prepare the polymer solution. Ethylene glycol (BDH Chemicals, AnalaR, 99.5%) was used as a non-solvent additive. Ethanol (GR grade, Merck, 99%) was used for the solvent exchange during spinning, and isopropyl alcohol (GR grade, Merck) was used as wetting liquid of the prepared PVDF membranes for the porosity measurements. PEG of molecular weight 35,000 was supplied from Fluka Chemika Co., and PEOs of various molecular weights were supplied from Aldrich Chemical Co.

2.2. Hollow fiber membrane preparation

Hollow fiber PVDF membranes were spun at room

Table 1
Hollow fiber spinning conditions and the resulting dimensions of the membranes

Membrane	Dope composition[a] (PVDF/EGL/DMAC) (wt%)	Internal coagulant (water/ethanol) (v/v%)	External coagulant (water/ethanol) (v/v%)	Internal diameter (mm)	External diameter (mm)	Wall thickness (mm)
4WW	23/4/73	100/0	100/0	1.33	1.60	0.14
4WE	23/4/73	100/0	50/50	1.33	1.66	0.17
4EW	23/4/73	50/50	100/0	1.19	1.57	0.19
4EE	23/4/73	50/50	50/50	1.15	1.49	0.17
6EE	23/6/71	50/50	50/50	1.16	1.44	0.14
8EE	23/8/69	50/50	50/50	1.10	1.39	0.15

[a] EGL refers to ethylene glycol and the spinning conditions are temperature, 20–22 °C; spinning pressure, 17.2 kPa; air gap, 25 cm; bore fluid flow rate, 0.1 ml/min.

temperature (20–22 °C) employing the solvent spinning technique. The spinning solutions were prepared from 23 wt% of PVDF in DMAC, and different concentrations of ethylene glycol (4, 6 and 8 wt%) in the spinning solution were considered. PVDF was dissolved in DMAC/ethylene glycol mixture and stirred at approximately 55 °C for about 12 h to ensure the complete dissolution of the polymer. The polymer dope prepared was transparent and homogenous at room temperature. The resulting solution was filtered through a 0.5 μm Teflon® filter, under a pressure of 2.41×10^5 Pa, to remove non-soluble contaminants. The mixture was then degassed overnight at room temperature. The spinning procedure was similar to the one described extensively by Kneifel and Peinemann [16]. In this process, the polymer solution was loaded into a reservoir and forced to the spinneret using pressurized nitrogen. The polymer solution and the internal coagulant liquid were pressed through a tube-in-orifice spinneret, in such a manner, that the polymer solution flowed through a ring nozzle while the coagulating fluid was fed through the inner tube. The polymer solution was directly extruded into a coagulation bath (i.e. external coagulant) that was placed at an air gap of 25 cm, under the spinneret and kept at room temperature. In this work, the bore liquid and the coagulation media were either distilled water or an aqueous ethanol solution (50% v/v). Spinning conditions were kept constant as follows. The pressure applied on the spinning solution was about 17.2 kPa and the bore liquid flow rate was kept at approximately 0.1 ml/min. After spinning, the hollow fibers were immersed in a coagulation bath at room temperature for at least 4 h. Furthermore, in order to prevent the shrinkage of the membranes during drying process, the prepared hollow fiber membranes were subjected to solvent exchange after coagulation. The membranes were immersed in pure ethanol for approximately 24 h. In this process, water in the membrane pores was replaced by ethanol that possesses lower surface tension. The membranes were subsequently dried in air at room temperature before characterization tests.

The inner and outer diameters of the prepared PVDF hollow fibers were measured by using a high resolution microscope (BHMJ Olympus BH2-UMA), with a precision of ±0.1 μm, on 10 different spots. The hollow fiber dimensions are shown in Table 1. The membrane modules are made of stainless steel with 0.7 cm inner diameter, 1 cm outer diameter, and 28 cm effective length. Each membrane module contains three fibers.

2.3. Hollow fiber membrane characterization

2.3.1. Liquid entry pressure of water measurements

Membrane LEPw is the pressure that must be applied onto distilled water before it penetrates into dried membrane pores. This pressure depends on the pore size and the hydrophobicity of the membrane. It decreases as the pore size increases and/or the contact angle decreases. The procedure to measure the LEPw of flat sheet membranes was extensively detailed elsewhere [12,17]. In this work, the same procedure is extended to the hollow fibers using the apparatus shown in Fig. 1. The lumen side of the module is connected to a container filled with distilled water. The container is pressurized with nitrogen and the pressure was read on a calibrated gauge. A digital capillary flowmeter (Varian Optiflow 420) was connected to the shell side of the membrane module. First, a slight pressure was applied to water for at least 10 min from a nitrogen cylinder; then the pressure was increased stepwise, with an increment of 0.68 kPa. Each pressure was kept at least for 30 min. The pressure at which a continuous flow is observed on the permeate side is the LEPw.

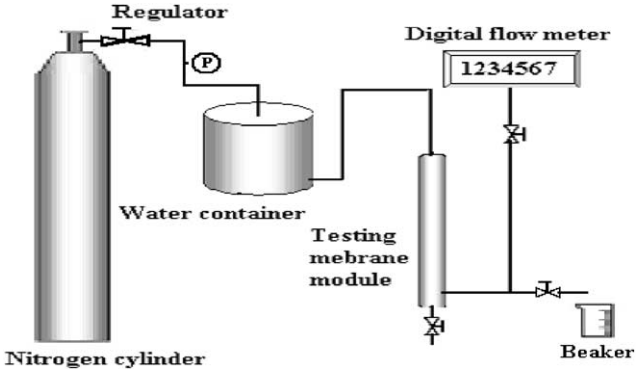

Fig. 1. Schematics of the experimental set-up used for the membrane liquid entry pressure of water (LEPw) measurement.

2.3.2. Hollow fiber membrane porosity measurement using isopropyl alcohol

The ratio between the volume of the pores and the total volume of the membrane is called the membrane porosity. This can be determined by measuring the density of the polymer material using isopropyl alcohol (IPA), which penetrates inside the pores of the membrane, and the density of the membrane using distilled water, which does not go into the pores. In this method, a pyknometer and a balance were employed and Eq. (1) can be used to determine the porosity [12,17]:

$$\varepsilon_v = 1 - \frac{\rho_m}{\rho_{pol}} \tag{1}$$

where ρ_m is the density of the membrane and ρ_{pol} is the density of the polymer material. More details concerning this method can be found elsewhere [17].

2.3.3. Gas permeation test

The mean pore size and the effective porosity of the prepared PVDF hollow fiber membranes were evaluated using the gas permeation method. The effective porosity is defined as the ratio of the porosity and the effective pore length that takes into account the tortuosity of the membrane pores. The experimental apparatus used is shown in Fig. 2. The lumen side of each membrane module was connected to a nitrogen cylinder. The permeation flux of nitrogen through the dried membranes was measured at various transmembrane pressures, from 0 to 206.84 kPa, at room temperature using a soap-bubble flowmeter when the gas flow rate was low and a wet flowmeter when the flow rate was high.

Generally, the gas permeance, B, for a porous medium may be expressed as a function of both the diffusive term and the viscous term that depends on the pressure as expressed by Carman [18] and used by most authors to test flat sheet or hollow fiber membranes [4,6,11,12]:

$$B = \frac{4}{3}\left(\frac{2}{\pi MRT}\right)^{0.5}\frac{r_p\varepsilon}{L_p} + \frac{P_m}{8\mu RT}\frac{r_p^2\varepsilon}{L_p} = I_0 + S_0P_m \tag{2}$$

where R is the gas constant, T the absolute temperature, M the molecular weight of the gas, μ the gas viscosity, P_m the mean pressure within the membrane pore, r_p the membrane pore radius, ε the porosity, L_p the effective pore length and ε/L_p is the effective porosity.

From the lineal plot between the permeance, B, and the pressure, P_m, the intercept (I_0) and the slope (S_0) can be determined and consequently the mean pore radius and the effective porosity can be calculated by using Eqs. (3) and (4):

$$r_p = \frac{16}{3}\left(\frac{S_0}{I_0}\right)\left(\frac{8RT}{\pi M}\right)^{0.5}\mu \tag{3}$$

$$\frac{\varepsilon}{L_p} = \frac{8\mu RT}{r_p^2}S_0 \tag{4}$$

This method was originally developed for symmetric membranes. In the case of composite membranes, the measured pore size corresponds to the global contribution, and for an asymmetric membrane with a skin layer the measured pore size is considered as a characteristic of the skin [4,6].

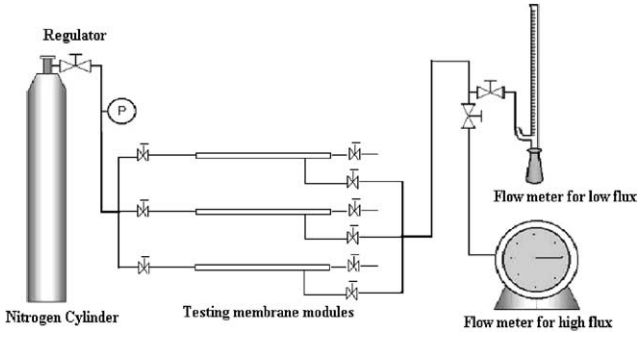

Fig. 2. Schematics of the experimental system used for the gas permeation test.

2.3.4. Scanning electron microscopy

The SEM is a powerful technique for analyzing the structure of the membranes. Due to the applied coating process, which induces some damage to the membrane, SEM is not a reliable method to measure the pore size. In this work, the cross-section of the PVDF hollow fibers membranes prepared with the method mentioned earlier was examined by a scanning electron microscope (SEM, JEOL Model JSM-6400). The samples were positioned on a metal holder and coated with 60% gold and 40% palladium under vacuum in a sputtering system HUMMER VII that provides a 2–3 nm conductive coating on the samples. The SEM pictures were taken over different regions of the same membrane at various magnifications.

2.3.5. Atomic force microscopy

AFM is a very useful method for studying the membrane surface structure. In this work, both the internal and the external surfaces of the PVDF hollow fibers were analyzed. AFM images were obtained over different areas of each hollow fiber membrane using a Nanoscope III from Digital Instruments Inc., Santa Barbara, CA. In order to analyze the internal surface of the hollow fiber membranes, the hollow fibers were cut longitudinally by means of a sharp razor blade and the samples were fixed over magnetic disks by using double side adhesive tape. The laser beam of the AFM was focused on the preselected spot of the surface prior to the engagement of the cantilever. A tapping mode, TM-AFM, in air was used to take the AFM images. The membrane pore sizes, nodule sizes and roughness parameters were therefore determined.

Mean pore size and pore size distribution. The measured pore sizes, from the line profiles on the AFM images with a scan size 0.1 μm × 0.1 μm, were arranged in ascending order and the median rank (50%), χ, was calculated using

Eq. (5) [19,20]

$$\chi = \left(\frac{i - 0.3}{n + 0.4}\right)100 \quad (5)$$

where i is the order number of the measured pore size arranged in ascending order and n is the total number of the measured pores.

If pore sizes have a log–normal distribution, the cumulative distribution function versus the ascending pore size must be a straight line on a log–normal probability paper. If this condition is satisfied, from the log–normal plot, the mean pore sizes and the geometric standard deviation can be calculated. The mean pore size will correspond to 50% of the cumulative number of pores and the geometric standard deviation can be calculated from the ratio of 84.13% of the cumulative number of pores to that of 50%. From the values of the mean pore size and the geometric standard deviation, the pore size distribution can be expressed by the probability density function described by the following equation [19]

$$\frac{df(d_p)}{d(d_p)} = \frac{1}{d_p \ln \sigma_p (2\pi)^{1/2}} \exp\left(-\frac{(\ln d_p - \ln \mu_p)^2}{2(\ln \sigma_p)^2}\right) \quad (6)$$

where d_p is the pore size, σ_p the geometric standard deviation and μ_p is the geometric mean pore size of the membrane.

Surface roughness. The difference in the membrane surface morphology can be expressed in terms of various roughness parameters, such as the mean roughness, R_a, the root mean-square of Z data, R_q, and the mean difference in the height between the five highest peaks and the five lowest valleys, R_z. Those parameters have been determined for the inner and the outer surfaces of the PVDF hollow fiber membranes from the AFM images scanned at 5 μm range.

The mean roughness, R_a, is the mean value of the surface relative to the central plane for which the volume enclosed by the images above and below this plane are equal. This parameter was calculated from Eq. (7)

$$R_a = \frac{1}{L_x L_y} \int_0^{L_x} \int_0^{L_y} |f(x,y)| dx\, dy \quad (7)$$

where $f(x,y)$ is the surface relative to the central plane and L_x and L_y are the dimensions of the surface.

The root mean-square roughness, R_q, is the standard deviation of the Z values within a given area and is given by Eq. (8)

$$R_q = \sqrt{\frac{\sum (Z_i - Z_m)^2}{N_p}} \quad (8)$$

where Z_i is the current Z value, Z_m the mean average of the Z values, and N_p is the number of points.

The average difference in height, R_z, between the five highest peaks and the five lowest valleys is calculated relative to the mean plane, which is a plane about which the image data has a minimum variance.

The roughness parameters obtained from AFM images should not be considered as absolute values because it depends on the treatment of the captured surface data (plane fitting, flattering, filtering, etc.).

Nodule size. The nodule sizes of the internal and the external surfaces of the PVDF hollow fiber membranes were measured by inspecting line profiles of different high peaks on the same AFM images used to determine the pore size.

2.3.6. Ultrafiltration experiments

The membranes were tested for ultrafiltration using PEG with molecular weight 35,000 g/mol and PEOs with different molecular weights (100,000, 200,000, 300,000 and 400,000 g/mol). The experimental device used is shown in Fig. 3. The experiments were conducted according to the method described by Liu et al. [21]. In this work, the feed temperature was maintained constant at 21–22 °C, the solute concentration at 200 ppm, the feed pressure at 482.63 kPa (gauge) (70 psi) when testing the membranes prepared with 4 wt% of ethylene glycol in the polymer solution and 344.74 kPa (50 psi) when testing the membranes prepared with 6 and 8 wt% of ethylene glycol in the polymer solution. Each membrane was initially subjected to pure water experiments to determine the pure water permeation flux (PWP). Then PEG and PEO aqueous solutions were circulated through the membrane modules for about 1.5 h. The product permeation rate (PR), in presence of solute as feed, was then determined. The solute concentration in the feed and in the permeate were measured by the total organic carbon (TOC) analyzer (Dohrmann DC-190, Folio Instruments), and the solute separation was calculated using the following equation:

$$\alpha = \left(1 - \frac{C_p}{C_f}\right)100 \quad (9)$$

where C_p and C_f are the solute concentration in the permeate and in the feed solution, respectively.

In ultrafiltration study, the Einstein–Stokes diameter is used as a parameter to characterize the size of the solutes. Singh et al. [19] have determined the Einsten–Stokes diameters of PEG and PEO solutes from their molecular

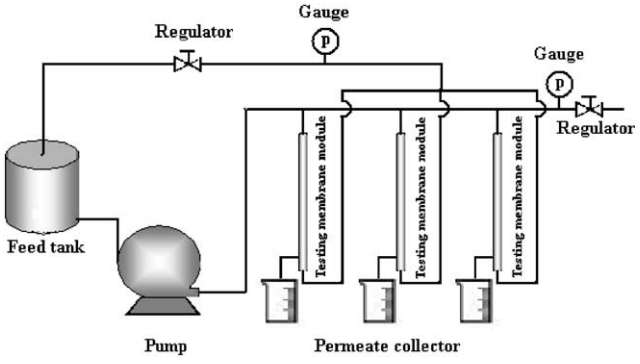

Fig. 3. Schematics of the experimental system used for ultrafiltration experiments.

weights using Eqs. (10) and (11), respectively:

$$a_d = 33.46 \times 10^{-10} M^{0.557} \quad (10)$$

$$a_d = 20.88 \times 10^{-10} M^{0.587} \quad (11)$$

where a_d is Einsten–Stokes diameter in cm, M is the molecular weight of the corresponding molecule in kg/kmol.

The mean pore size and the corresponding geometric standard deviation can be then determined from the solute transport data as follows: the solute separations and the corresponding Einsten–Stokes diameters are plotted on a log–normal probability paper. A straight line must be obtained. The Einsten–Stokes diameter that corresponds to 50% of the separation factor is considered the mean pore size, while the ratio between the Einsten–Stokes diameter corresponding to 84.13% of the separation factor and that corresponding to 50% is considered the geometric standard deviation.

The pore density, N, defined as the number of pores per unit membrane area can be calculated from the permeability data using the following expression based on the Hagen–Poisseuille equation [19].

$$N = \frac{128 \eta \delta J}{\pi \Delta P \sum_{d_{min}}^{d_{max}} f_i d_i^4} \quad (12)$$

where δ is the length of the pores assumed to be equal to the thickness of the membrane, η the solvent viscosity, ΔP the pressure difference across the membrane pores, J the total flux through the membrane, and f_i is the fraction of the number of pores with the diameter d_i.

The surface porosity, defined as the ratio between the area of the pores to the total membrane surface area, can be calculated from Eq. (13) [19]:

$$\varepsilon_s = \left(\frac{N\pi}{4} \sum_{d_{min}}^{d_{max}} f_i d_i^2 \right) 100 \quad (13)$$

3. Results and discussion

3.1. Membrane liquid entry pressure of water measurement

The obtained LEPw values of the prepared PVDF hollow fiber membranes are presented in Table 2. For the same content of the non-solvent additive (4 wt%) in the PVDF spinning solution, the LEPw decreases as ethanol (50% v/v) was added to the bore liquid and/or to the coagulation bath. The smallest LEPw is obtained when ethanol is present in the internal and in the external coagulants. Moreover, it seems that the effect of ethanol is stronger when it was added to the internal coagulant. In comparison with the hollow fiber membranes spun with water as internal and external coagulants, the LEPw decreased by 10.8% for 50% ethanol as internal coagulant, while it decreased only by 3.1% for 50% ethanol in the external coagulation media. It was also found that the LEPw decreased as the concentration of ethylene glycol increased in the PVDF spinning solution. The decrease of LEPw is due to the increase in the pore size (i.e. maximum pore size) of the membranes. Therefore, it can be concluded that the pore size of the PVDF hollow fiber membranes increases with an increase in the concentration of ethylene glycol and also when ethanol was added to either the bore liquid or to the coagulation bath or both.

Table 2
Liquid entry pressure of water (LEPw), membrane porosity measured using isopropyl alcohol (ε_v) and the results of the gas permeation test of the prepared PVDF hollow fiber membranes

Membrane	LEPw (kPa)	ε_v (%)	Gas permeation test	
			r_p (nm)	ε/L_p (m^{-1})
4WW	448.16	26.55	12.99	1787.60
4WE	434.37	28.71	17.89	1190.40
4EW	399.90	32.07	21.95	872.39
4EE	379.21	33.19	23.51	980.29
6EE	137.89	39.46	28.42	1203.73
8EE	110.32	42.98	35.62	1021.16

It should be mentioned that, under the spinning conditions employed in this work, for the polymer solutions containing 6 and 8 wt% of ethylene glycol, circular hollow fibers could not be spun when using water as internal and external coagulant.

3.2. Membrane porosity measurement using isopropyl alcohol

The values of the membrane porosity obtained experimentally by using isopropyl alcohol are also shown in Table 2. In general, in comparison to the membrane 4WW, the membrane porosity increased as ethanol was added to either the bore liquid and/or to the coagulation medium. This may be attributed to the elimination of skin layer when ethanol was added to the coagulant suggested by Deshmukh and Li [6] and by Wang et al. [7], or to the increase of pore size as concluded from the LEPw measurements. Moreover, when a water/ethanol mixture (50% v/v) was employed as an internal and an external coagulant, the porosity also increased with an increase in the concentration of ethylene glycol. Consequently, the pore size and the porosity of the prepared hollow fiber membranes increase with the addition of ethanol either in the bore fluid and/or in the coagulation bath and also with an increase in the concentration of ethylene glycol in the polymer solution.

3.3. Gas permeation test

The prepared PVDF hollow fiber membranes were characterized by the gas permeation test in order to determine the mean pore size and the effective porosity. The obtained results are shown in Table 2. It can be noticed

that the mean pore size becomes larger with the addition of ethanol either in the bore liquid and/or in the coagulation bath. Furthermore, as the concentration of ethylene glycol in the PVDF spinning solution increases the pore size increases. This observation is in agreement with the earlier results obtained from the LEPw measurements. However, in comparison with the hollow fiber spun with water as internal and external coagulant, the effective porosity decreases with the addition of ethanol in the coagulation bath and in the bore liquid solution. This is a trend opposite to the one observed in the porosity measurement using isopropyl alcohol. This may be due to the increase in the formation of dead-end pores, which increases the porosity (ε_v) as isopropyl alcohol penetrates through both the opened pores and the dead-ended pores. Furthermore, Deshmukh and Li [6] found that the effective porosity of PVDF hollow fiber membranes, prepared with 4 wt% of PVP as non-solvent additive, decreased as ethanol concentration in the coagulation bath was increased. However, Wang et al. [7] observed that the effective porosity of the PVDF hollow fiber membranes prepared with PVP as non-solvent additive and using ethanol as internal coagulant was larger than that of the membranes prepared using water as internal coagulant. Deshmukh and Li [6] and Wang et al. [7] attributed those results to the slow polymer precipitation that occurred when ethanol was added to the coagulant and eliminated the skin layer. Therefore, the result is an increase of the effective pore length (L_p) and an increase in the formation of dead-end pores, which decreases the porosity (ε). These two effects would either increase or decrease the effective porosity depending on which is the dominating factor. In addition, when ethanol was added in both the internal and the external coagulants, the largest effective porosity was obtained when the dope solution was prepared from 6 wt% of non-solvent additive (i.e. membrane 6EE). The effective porosity was almost the same for both the hollow fiber membranes prepared from 4 and 8 wt% of the non-solvent additive in the spinning solution.

3.4. Scanning electron microscopy

Fig. 4(a)–(d) show the cross-sectional structures of the PVDF hollow fibers prepared from 4 wt% of ethylene glycol in the PVDF spinning solution under four coagulation conditions. As can be seen, those figures exhibit different internal structures. In Fig. 4(a) that corresponds to the membrane prepared with water as internal and external coagulants, long finger-like voids are formed near the inner wall, while there is formation of smaller cavities near the outer wall. Between the inner and the outer layers sponge-like structure appears. Fig. 4(b) reveals that the inner layer was reduced when ethanol was added to the internal coagulant, while Fig. 4(c) shows that the outer layer has been eliminated when ethanol was added to the coagulation bath and a uniform sponge-like structure extends over the entire membrane cross-section when

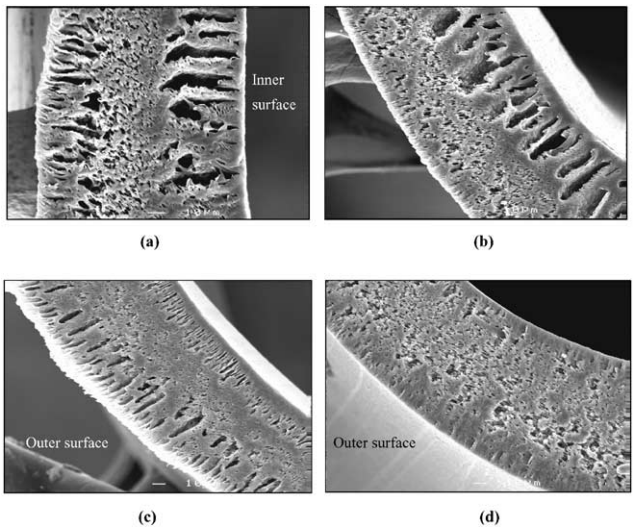

Fig. 4. Cross-sectional SEM pictures of PVDF hollow fiber membranes. (a) 4WW membrane, (b) 4WE membrane, (c) 4EW membrane, and (d) 4EE membrane.

ethanol was added to both the internal and the external coagulant (Fig. 4(d)). Hence, the structure of PVDF membranes is largely dependent on the nature of the coagulants. For PVDF, water is a strong non-solvent. This means that coagulation takes place fast when the polymer solution is brought into contact with water. As reported by Kesting [22], generally large finger-like macrovoids and cavity-like structures are formed when the coagulation process is fast, whereas the slow coagulation rate results in a porous sponge-like structure. Ethanol is not as strong a non-solvent as water. This indicates that the addition of ethanol will delay the coagulation process and a long finger-like structure will change to a short finger-like structure and further to a sponge-like structure. On the other hand, the solubility parameter difference between water (47.8 $J^{1/2}/cm^{3/2}$) and the solvent DMAC (22.7 $J^{1/2}/cm^{3/2}$) is about 1.7 times higher than the solubility parameter difference between an aqueous solution of 50% ethanol (37.2 $J^{1/2}/cm^{3/2}$) and DMAC [6]. It is known that the higher is the solubility parameter difference, the lower is the affinity between the components. This indicates that the rate of mixing between DMAC and water is higher than between DMAC and an aqueous solution of 50% ethanol. Deshmukh and Li [6] and Bottino et al. [15] explained the slow precipitation on the basis of the solvent/non-solvent mutual diffusivity between DMAC, ethanol and water. In fact, the diffusion coefficient of water in DMAC is 1.68×10^{-5} cm^2/s while the diffusion coefficient of ethanol in DMAC is lower, 0.04×10^{-5} cm^2/s [6]. Consequently, the effect of the addition of ethanol either into the external and/or the internal coagulant is to decrease the diffusion of non-solvent into the forming fiber and thus reduces the rate of precipitation. It must be mentioned that the cross-sectional SEM pictures of the hollow fibers prepared with 4, 6 and 8 wt% of ethylene glycol as non-solvent additive were almost the same when the water/ethanol mixture (50%

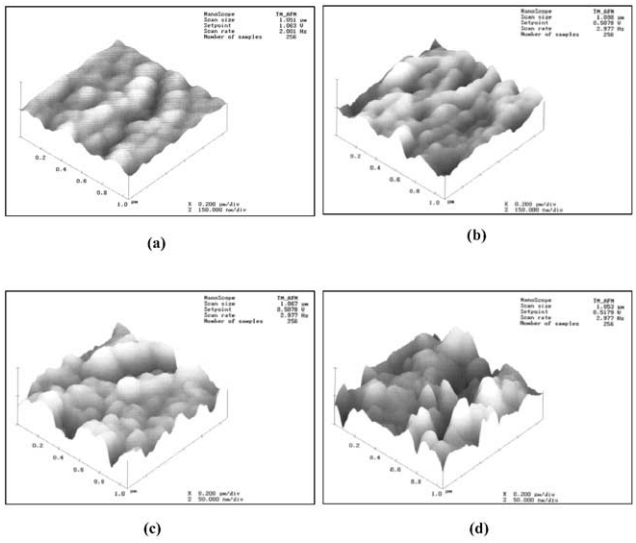

Fig. 5. Atomic force microscopic images of the inner and the outer surfaces of PVDF hollow fiber membranes 4WW and 8EE. (a) Inner 4WW membrane, (b) inner 8EE membrane, (c) outer 4WW membrane, and (d) outer 8EE membrane.

v/v) was used as internal and external coagulant (i.e. sponge-like structure).

3.5. Atomic force microscopy

Fig. 5 shows, as an example, the AFM images of the inner and the outer surfaces of the hollow fibers 4WW and 8EE. The images are presented in 1000 nm × 1000 nm scanning area with a 150 nm Z range for the inner surfaces, while for the outer surfaces the images are presented in 1000 nm × 1000 nm scanning area with a 50 nm Z range. As expected, a difference in the morphology of the PVDF hollow fiber membranes can be observed. The AFM images revealed that surfaces of the membranes are not smooth and the nodule-like structure and the nodule aggregates are present, at both the inner and the outer surfaces of the PVDF hollow fibers, as defined by Kesting [22]. The nodules are characterized by the high peaks seen as bright regions in the AFM pictures. Table 3 shows the minimum, maximum and the average nodule sizes of both the inner and the outer surfaces. Feng et al. [20] reported that the nodule size of the inner surface of polyetherimide (PEI) hollow fibers was smaller than the nodule size of the outer surface. In the present study, the average nodule size of the inner surface is higher than that of the outer surface for all membranes except for the membrane 8EE. This may be due to the difference in polymer type or in spinning conditions.

The roughness parameters of the inner and the outer surfaces of the PVDF hollow fiber membranes are also given in Table 3. It should be mentioned that the roughness parameters were calculated in AFM scanning area of 5 μm × 5 μm. From the obtained data presented in Table 3, it can be noticed that the roughness parameters for the membranes prepared with 4 wt% of the non-solvent additive in the spinning solution increase on the membrane side that is in contact with ethanol solution. Generally, the membrane roughness became higher when ethanol was added in the coagulant. This may be due to the increase of the pore size and the porosity. Singh et al. [19], Bessieres et al. [23] and Fritzsche et al. [24] reported that the change in the roughness parameters is proportional to the change in the pore size. This may be explained since the roughness parameters depend on the Z values. When the surface consists of deep depressions that characterize pores and high peaks that correspond to nodules, high roughness parameters are expected. Interestingly, however, the highest roughness parameters of the inner and the outer surfaces were obtained for the membrane 6EE. The pore size of this membrane is smaller than the pore size of the membrane 8EE that has lower roughness parameters. This may be due to the influence of the porosity, which is higher for this membrane in comparison to the membrane 8EE.

Table 3
Results of the AFM analysis of the inner and the outer surfaces of the PVDF hollow fiber membranes

Membrane	Surface	μ_p (nm)	σ_p	Nodule sizes[a]			Roughness parameters		
				ν_L (nm)	ν_m (nm)	ν_H (nm)	R_a (nm)	R_q (nm)	R_z (nm)
4WW	Inner	70.16	1.10	41.06	96.95	147.83	10.02	12.84	78.69
	Outer	50.47	1.16	41.68	85.06	137.55	7.90	10.26	67.87
4WE	Inner	79.88	1.20	70.69	150.71	278.83	9.40	11.68	75.31
	Outer	66.57	1.17	50.21	137.72	343.10	13.54	16.65	97.04
4EW	Inner	78.42	1.13	55.12	132.71	240.14	13.12	16.12	114.29
	Outer	57.32	1.17	40.20	124.24	313.59	11.26	14.88	121.51
4EE	Inner	91.38	1.20	61.20	153.19	297.82	17.23	22.29	137.05
	Outer	82.03	1.22	42.73	135.42	286.25	14.98	19.03	126.79
6EE	Inner	131.84	1.27	95.80	174.16	258.23	48.40	60.28	417.34
	Outer	112.36	1.23	39.06	123.70	285.16	81.93	110.8	1149.0
8EE	Inner	157.57	1.23	68.61	134.61	287.31	33.01	40.39	379.02
	Outer	142.97	1.29	49.36	145.35	300.29	31.84	41.77	549.75

[a] ν_L: minimum nodule size; ν_m: average nodule size; ν_H: maximum nodule size.

The pores were characterized by the deep depressions seen as dark regions in the pictures. Different pore shapes were observed in the AFM images of the inner and the outer surfaces of the PVDF hollow fibers. The pore sizes were therefore determined from the average size of the length and the width of the pores. The median ranks were plotted as a function of the measured pore sizes on a log–normal probability paper. Straight lines have been fitted to the data with reasonably high correlation coefficient ($r^2 \geq 0.93$) for the inner and the outer surfaces of all prepared membranes. As an example, Fig. 6 shows the log–normal pore size distribution of the inner and the outer surfaces of the membranes 4WE and 6EE. The mean pore size and the geometric standard deviation of the inner and the outer surfaces were calculated according to the method explained previously. The results are presented in Table 3 for both the inner and the outer surfaces. It can be noticed that, for all prepared PVDF hollow fiber membranes, the pores at the inner surface are larger than those at the outer surface and the pore size increases simultaneously at the inner and at the outer surfaces as ethanol was added to the coagulants and also with the increase of the concentration of the non-solvent in the spinning solution. The internal and the external mean pore sizes determined by AFM have the same trend as the pore size determined by the gas permeation test. Nevertheless, the inner and the outer pore sizes determined by AFM were, respectively, about 2.2 and 1.8 times larger than those calculated from the gas permeation test. This is probably because the pores measured by AFM have maximum openings at the surface entrance.

The cumulative pore size distribution curves and the probability density function curves for the inner and the outer surfaces were generated from the values of the mean pore size and the geometrical standard deviation [19]. Figs. 7 and 8 show the results for both the inner and the outer surfaces of the prepared PVDF hollow fiber, respectively. In comparison to the membrane 4WW, the pore size distribution curves shift to the right when ethanol is added either in the internal or the external coagulant, and also with an increase of ethylene glycol content in the polymer solution.

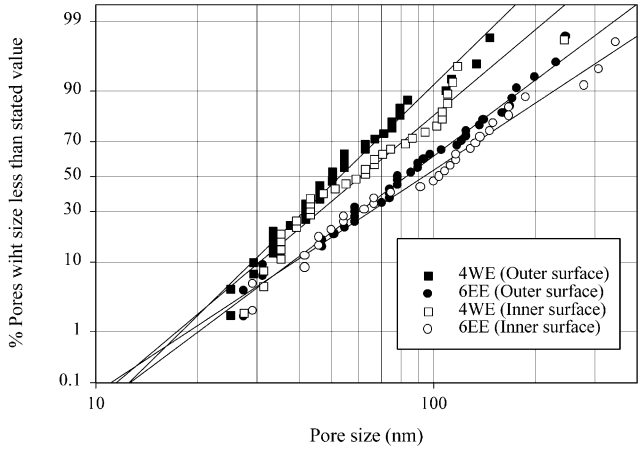

Fig. 6. Log–normal pore size distributions of the pore sizes measured from the AFM images of the inner and the outer surfaces of PVDF hollow fiber membranes.

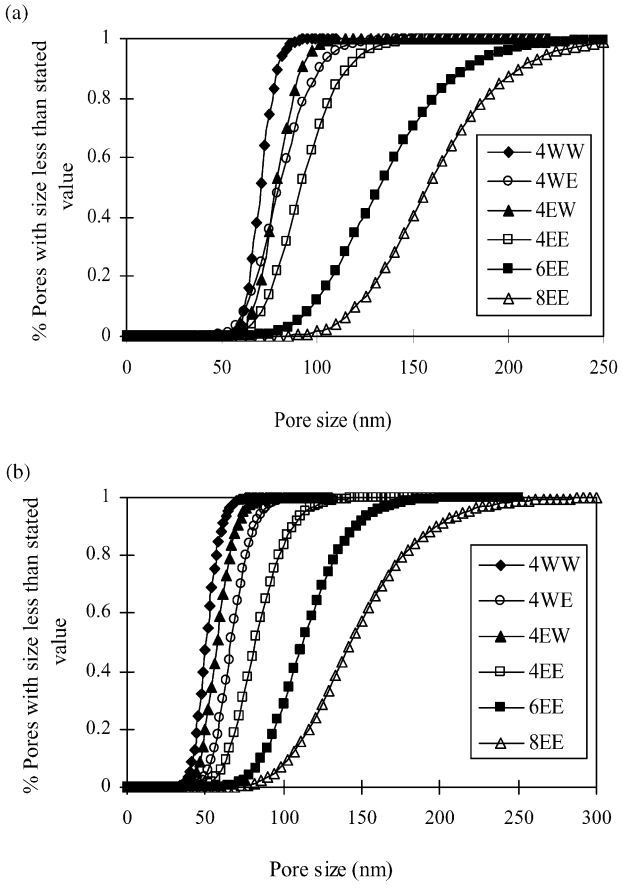

Fig. 7. Cumulative distributions of the pore sizes measured from the AFM images of the (a) inner and (b) outer surfaces of PVDF hollow fiber membranes.

3.6. Ultrafiltration experiments

The results of ultrafiltration experiments are summarized in Table 4. Prior to the solute transport experiment, the PWP flux was measured. It can be seen that the PWP flux increases with the addition of ethanol either in the internal or the external coagulant and also it increases with an increase in the concentration of the non-solvent. This is not unexpected when the change in the pore size is considered. It can also be observed that the PWP flux is higher when ethanol was added to the internal coagulant than to the coagulation bath.

The PR was determined in the presence of PEG (35,000 g/mol) and the results are shown in Table 4. The PR values are lower than the PWP. The ratio between PR and PWP varies between 0.66 and 0.74.

On the other hand, for both PEG and PEO tested, the solute separation decreased with an increase of ethylene glycol concentration in the PVDF spinning solution and when ethanol is added to either the bore liquid or to the

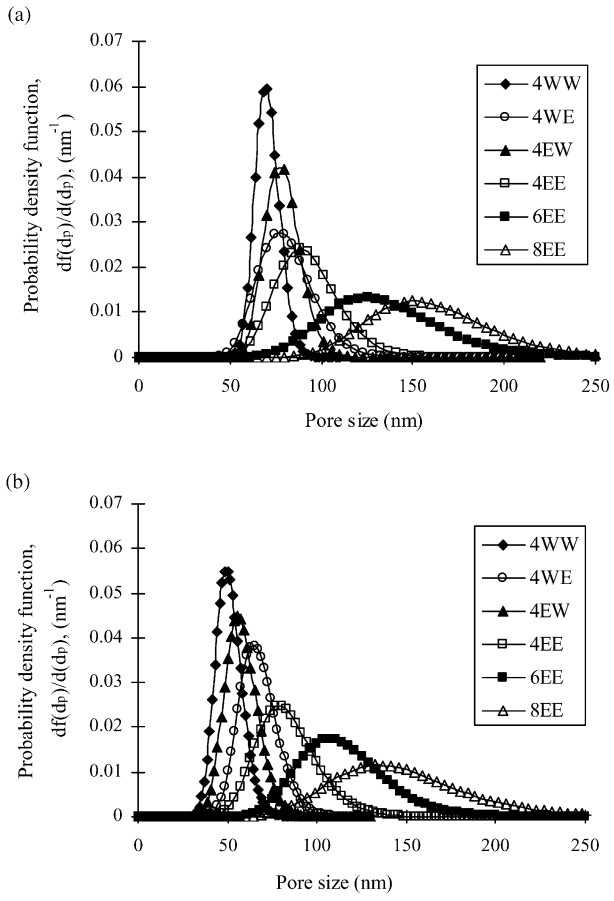

Fig. 8. Probability density function curves generated from the pore sizes measured from the AFM images of the (a) inner and (b) outer surfaces of PVDF hollow fiber membranes.

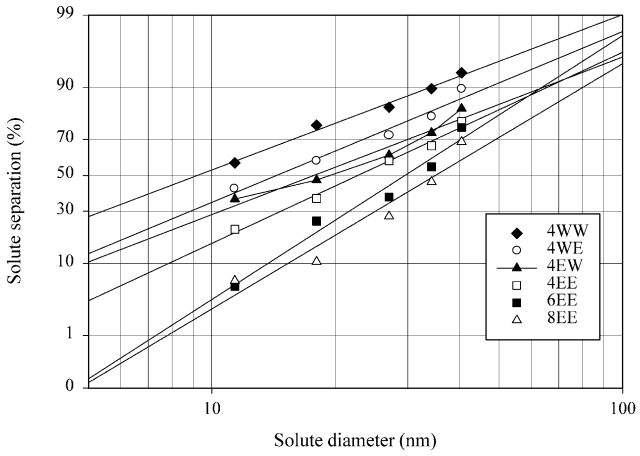

Fig. 9. Solute separation curves plotted on a log–normal probability paper for PVDF hollow fiber membranes.

coagulation bath or both. These results also mean that the pore size is increased with the concentration of ethylene glycol in the spinning solution and when ethanol was added to the internal or the external coagulant or both.

The pore sizes and the pore size distributions of the membranes were further determined based on the solute transport data given in Table 4. In Fig. 9, the percent solute separation was plotted as a function of the Einstein–Stokes diameters of solutes on a log–normal probability paper. Straight lines could fit the data with reasonably high correlation coefficients ($r^2 \geq 0.93$). The different slopes of the lines indicate the different pore size distribution of the different prepared PVDF hollow fibers. The mean pore size and the geometric standard deviation were then determined from the straight lines in Fig. 9. The results are shown in Table 5.

The geometric standard deviations of the membranes are very close to each other (from 1.23 to 1.42), while the mean pore size increases when ethanol is added to the coagulant and when the concentration of ethylene glycol is increased in the spinning solution. The same trend is observed as in the gas permeation test and AFM analysis. The mean pore size determined by the gas permeation test is about 1.5 times higher than the pore size determined from the solute transport data, while the pore size determined by AFM analysis is about three times larger than the pore size determined by the solute transport experiments. Recently, Singh et al. [19] concluded that the pore sizes measured by AFM were about 3.5 times larger than those calculated from the solute transport, after testing various ultrafiltration and nanofiltration membranes. Bessieres et al. [23] also observed that

Table 4
Results of the ultrafiltration experiments of the PVDF hollow fiber membranes

Membrane	PWP (10^{-6} m^3/m^2 s)	PR[a] (10^{-6} m^3/m^2 s)	Solute separation (%)				
			PEG, 35,000 (g/mol)	PEO			
				100,000 (g/mol)	200,000 (g/mol)	300,000 (g/mol)	400,000 (g/mol)
4WW	24.25	17.56	57.2	76.7	83.9	89.6	93.2
4WE	24.75	16.25	42.3	58.6	71.8	80.5	89.7
4EW	32.36	21.22	36.5	47.3	61.6	73.2	83.4
4EE	34.28	22.58	21.6	36.9	58.4	66.7	78.3
6EE	41.00	29.86	5.3	25.3	37.6	54.9	75.8
8EE	46.64	34.61	6.3	10.5	27.6	46.3	68.7

[a] Product permeation rate measured with PEG of molecular weight 35,000 g/mol.

Table 5
Mean pore size (μ_p), geometric standard deviation (σ_p), pore density (N), surface porosity (ε_s) and the molecular weight cut-off (MWCO) of the PVDF hollow fiber membranes calculated from the solute transport

Membrane	μ_p (nm)	σ_p	N (μm^{-2})	ε_s (%)	MWCO (kDa)
4WW	15.36	1.42	1575.31	40.60	153.3
4WE	22.85	1.37	495.35	26.37	283.1
4EW	29.30	1.41	237.59	21.71	455.7
4EE	34.28	1.33	162.18	18.70	528.5
6EE	39.81	1.23	119.44	23.96	583.2
8EE	48.40	1.25	62.41	18.56	839.5

AFM gave two to four times bigger diameters than those obtained from the solute transport.

In addition, the molecular weight cut-off (MWCO) of the membranes was calculated based on 90% separation by the membrane. From the log–normal probability plot, the solute diameter corresponding to 90% separation can be obtained, and then by using the empirical equations (Eqs. (10) and (11)) the molecular weight can be further calculated. In general, the mean pore size has the same trend as the MWCO. It increases with the addition of ethanol either in the internal or in the external coagulant or both and with the concentration of ethylene glycol in the polymer solution. The mean pore size is higher for the membranes having higher MWCO.

The cumulative pore size distributions and the probability density function curves are shown in Fig. 10. Those were determined by using the values of mean pore size and geometric standard deviation. It is evident from this figure that there is a change in pore size distributions of the prepared PVDF hollow fiber membranes. There is a rightward shift of both the cumulative pore size and the probability density as ethanol was added either to the internal or to the external coagulant or both and also with the increase of the ethylene glycol content in the polymer solution.

The pore density and surface porosity were calculated from Eqs. (12) and (13), respectively, and the results are also shown in Table 5. Both, the pore density and the surface porosity decrease with an increase of the concentration of the non-solvent additive in the spinning solution and when ethanol was added either in the internal or the external coagulant or both. As the pore size increases the pore density and the surface porosity decrease. However, the PWP flux increases. This indicates that the pore size has a predominant effect on the permeation under the experimental conditions used in the present study.

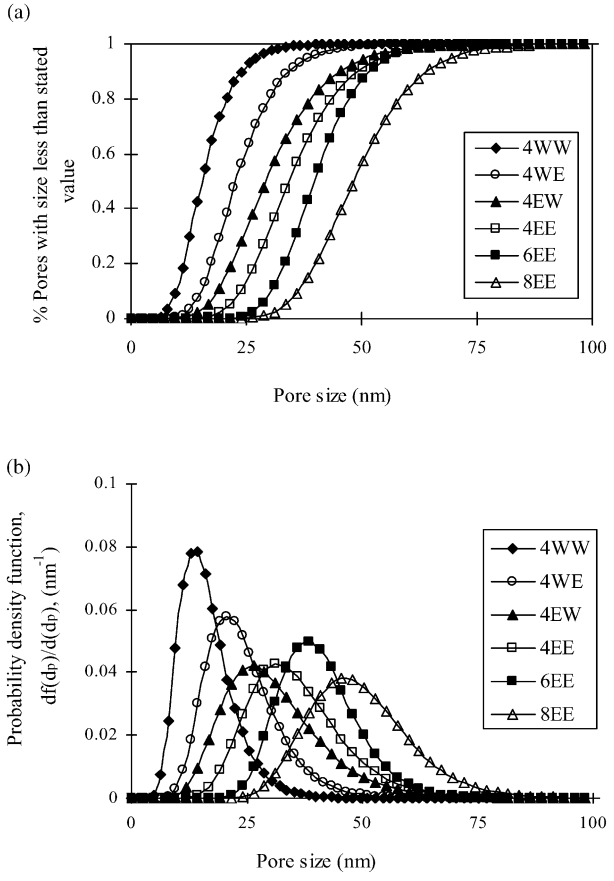

Fig. 10. (a) Cumulative pore size distributions and (b) probability density function curves for PVDF hollow fiber membranes determined from solute transport experiments.

4. Conclusions

PVDF hollow fiber membranes with different pore sizes were spun using the solvent spinning method. The polymer solutions were prepared from 23 wt% of PVDF in DMAC employing different concentrations of ethylene glycol (4, 6 and 8 wt%) as non-solvent additive. The membranes so prepared were characterized by various methods. The LEPw to dried membrane pores, the membrane porosity using isopropyl alcohol, the gas permeation test employing nitrogen to determine the mean pore size and the effective porosity which takes into account the pore tortuosity, the SEM, the AFM and ultrafiltration experiments using PEG and PEOs of different MWCO as solutes. It was observed that:

1. The pore sizes determined by AFM, gas permeation test and solute transport experiment, all increased as the concentration of ethylene glycol in the spinning solution increased and when ethanol was added to either the internal or the external coagulant or both.
2. From AFM studies, the pore size of the inner surface was larger than the pore size of the outer surface.
3. The mean pore size determined by AFM was about two times larger than the pore size determined by the gas permeation test (i.e. ≈2.2 for the inner pore size and ≈1.8 for the outer pore size) and was about three times larger than that calculated from the solute transport experiments (i.e. ≈3.3 for the inner pore size and ≈2.7 for the outer pore size).
4. The effective porosity determined by the gas permeation

test decreased with the addition of ethanol in either the bore liquid or in the coagulation bath or both. The same trend was observed when the surface porosity was determined by the solute transport experiments.

5. Nodules and nodule aggregates were observed at the inner and at the outer surfaces of the prepared PVDF hollow fiber membranes.
6. Cross-sectional SEM pictures revealed that finger-like structures were formed when water was used as coagulant, whereas a sponge-like structure appeared when a water/ethanol mixture (50% v/v) was used either as internal or external coagulant.

Acknowledgements

The authors of this work gratefully acknowledge the postdoctoral research grant provided by the University Complutense of Madrid to Dr Mohamed Khayet. They are also thankful for the support by the Natural Sciences and Engineering Council of Canada and Petrosep Membrane Technologies Co. through Collaborative Research and Development Grant.

References

[1] Ortiz de Zarate JM, Pena L, Mengual JI. Desalination 1995;100:139.
[2] Tomaszewska M. Desalination 1996;104:1.
[3] Jian K, Pintauro PN. J Membrane Sci 1994;135:41.
[4] Li K, Kong JF, Wang D, Teo WK. AIChE J 1999;45(6):1211.
[5] Bottino A, Capannelli G, Munari S, Turturro A. Desalination 1988;68:167.
[6] Deshmukh SP, Li K. J Membrane Sci 1998;150:75.
[7] Wang D, Li K, Teo WK. J Membrane Sci 1999;163:211.
[8] Uragami T, Naito Y, Sugihara M. Polym Bull 1981;4:617.
[9] Uragami T, Fujimoto M, Sugihara M. Desalination 1980;34:311.
[10] Shih HC, Yeh YS, Yasuda H. J Membrane Sci 1990;50:299.
[11] Wang D, Li K, Teo WK. J Membrane Sci 2000;178:13.
[12] Khayet M, Takeshi M. Ind Eng Chem Res 2001;40:5710.
[13] Benzinger WD, Robinson DN. United States Patent 4,384,047, 1998.
[14] Bottino A, Capannelli G, Munari S. J Appl Polym Sci 1985;30:3009.
[15] Bottino A, Camera-Roda G, Capannelli G, Munari S. J Membrane Sci 1991;57:1.
[16] Kneifel K, Peinemann KV. J Membrane Sci 1992;65:295.
[17] Smolder K, Franken ADM. Desalination 1989;72:249.
[18] Carman PC. Flow of gases through porous media. London: Butterworths, 1956.
[19] Singh S, Khulbe KC, Matsuura T, Ramamurthy P. J Membrane Sci 1998;142:111.
[20] Feng CY, Khulbe KC, Chowdhury G, Matsuura T, Sapkal VC. J Membrane Sci 2001;189:193.
[21] Liu T, Xu S, Zhang D, Sourirajan S. Desalination 1991;85:1.
[22] Kesting RE. Synthetic polymeric membranes. 2nd ed. New York: Wiley, 1985.
[23] Bessieres A, Meireles M, Cortger R, Beauvillain J, Sanchez V. J Membrane Sci 1996;109:271.
[24] Fritzche AK, Arevalo AR, Moor MD, Weber CJ, Elings VB, Kjoller K, Wu MC. J Appl Polym Sci 1992;46:167.